Supplementary information

Ultrathin two-dimensional π-d conjugated coordination polymer Co_3(hexaaminobenzene)$_2$ nanosheets for highly efficient oxygen evolution

Chun Li[†], *Lingling Shi*[†], *Lili Zhang*[‡], *Peng Chen*[†], *Junwu Zhu*[†], *Xin Wang**[†], *and Yongsheng Fu**[†]

[†]Key Laboratory for Soft Chemistry and Functional Materials of Ministry of Education, Nanjing University of Science and Technology, Nanjing 210094, China

[‡]Jiangsu Key Laboratory for Chemistry of Low-Dimensional Materials, Huaiyin Normal University, Huai'an, Jiangsu 223300, China

* Corresponding authors

E-mail addresses: fuyongsheng0925@163.com, fuyongsheng@njust.edu.cn (Y. S. Fu), wangx@njust.edu.cn (X. Wang)

Theoretical methods

Computational details and modeling

The density-functional theory (DFT) calculations in this work were performed using the Vienna Ab-initio Simulation Package (VASP) [1, 2]. The Blöchl's all-electron-like projector augmented plane wave (PAW) method was used to describe the interactions between ion cores and valence electrons [3, 4]. The electron exchange-correlation interaction was treated using the generalized gradient approximation (GGA) with the Perdew-Burke-Ernzerhof (PBE) functional.

A Hubbard-U correction (DFT+U method) was applied in the simulations, in order to improve the on-site Coulomb interactions for Co_3HAB_2. In the present work, the value of U is 0.4 and 0.72 for Co, respectively. The plane waves with a cutoff energy of 500 eV were used, and the 4×4×1 Monkhorst–Pack grid k-points were employed to sample the Brillouin zone integration. The structures were optimized until the energy and the force were converged to 1.0×10^{-5} eV/atom and 0.02 eV/Å, respectively. A vacuum space as large as 15 Å was used along the c direction normal to the catalyst surface to avoid periodic interactions.

OER reaction pathways

The general OER mechanism is the four electron associative pathway as described as follows:

$$OH^- + * \rightarrow OH^* + e^- \quad \text{(S1)}$$

$$OH^* + OH^- \rightarrow O^* + H_2O(l) + e^- \quad \text{(S2)}$$

$$O^* + OH^- \rightarrow OOH^* + e^-$$

(S3)

$$OOH^* + OH^- \rightarrow * + O_2 + H_2O(l) + e^-$$

(S4)

Derivation of free energy

The free energies were calculated from total energies using Eq. (S5).

$$\Delta G_i = \Delta E_i + \Delta ZPE_i - T\Delta S_i \quad \text{(S5)}$$

Where i = 1, 2, 3, 4 corresponds to each step in OER. ΔE is the reaction energy, ΔZPE is the change of zero-point energy, T (298.15 K) is temperature, and ΔS is the difference in entropy. The zero-point energies were calculated from the vibration frequencies. The entropies were taken from standard tables for gas-phase molecules.

Free energy diagram (FED) and overpotential (η)

The ΔG value of the potential-determining step (G^{OER}) in OER pathway was determined by Eq. S6:

$$G^{OER} = max[\Delta G_1, \Delta G_2, \Delta G_3, \Delta G_4]^0 \quad \text{(S6)}$$

The theoretical overpotential at standard conditions was calculated by Eq. (S7):

$$\eta^{OER} = (G^{OER}/e) - 1.23V \quad \text{(S7)}$$

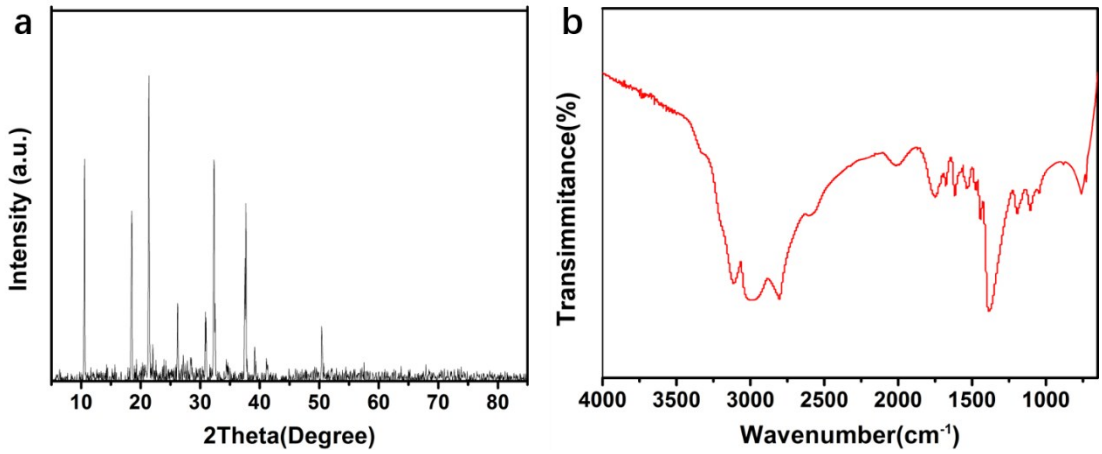

Figure S1. (a)XRD pattern and (b) IR spectra of HAB.

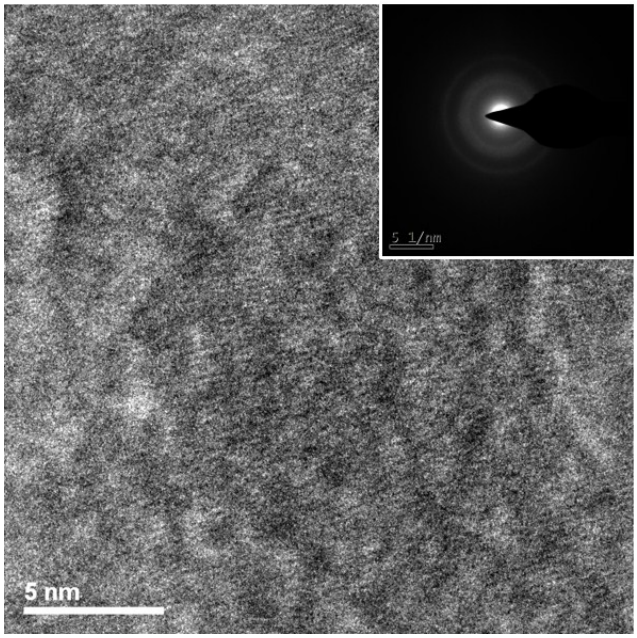

Figure S2 High resolution TEM image and selected-area electron diffraction of Co-HAB-NSs-2.

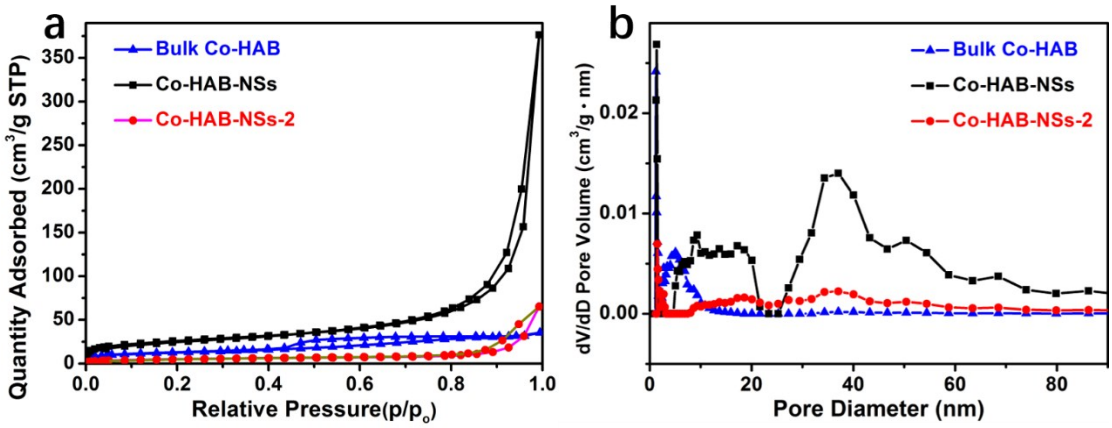

Figure S3. (a) Nitrogen adsorption-desorption isotherms and (b) pore size distribution of Co-HAB-NSs and Bulk Co-HAB.

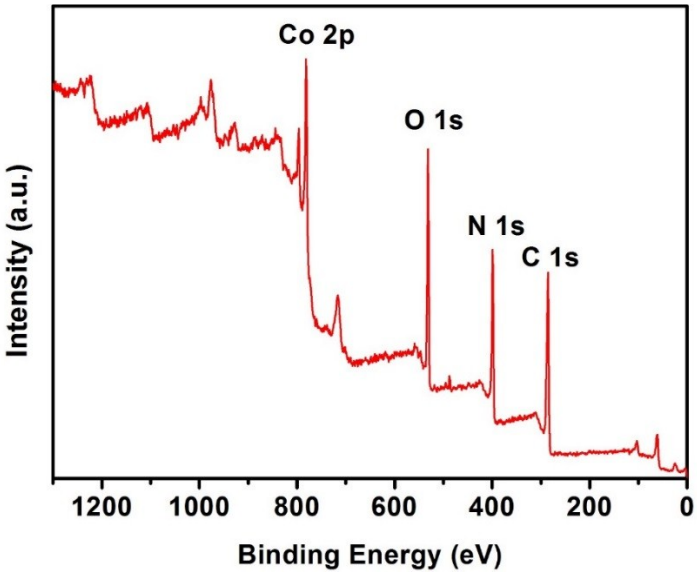

Figure S4. XPS spectrum of Co-HAB-NSs.

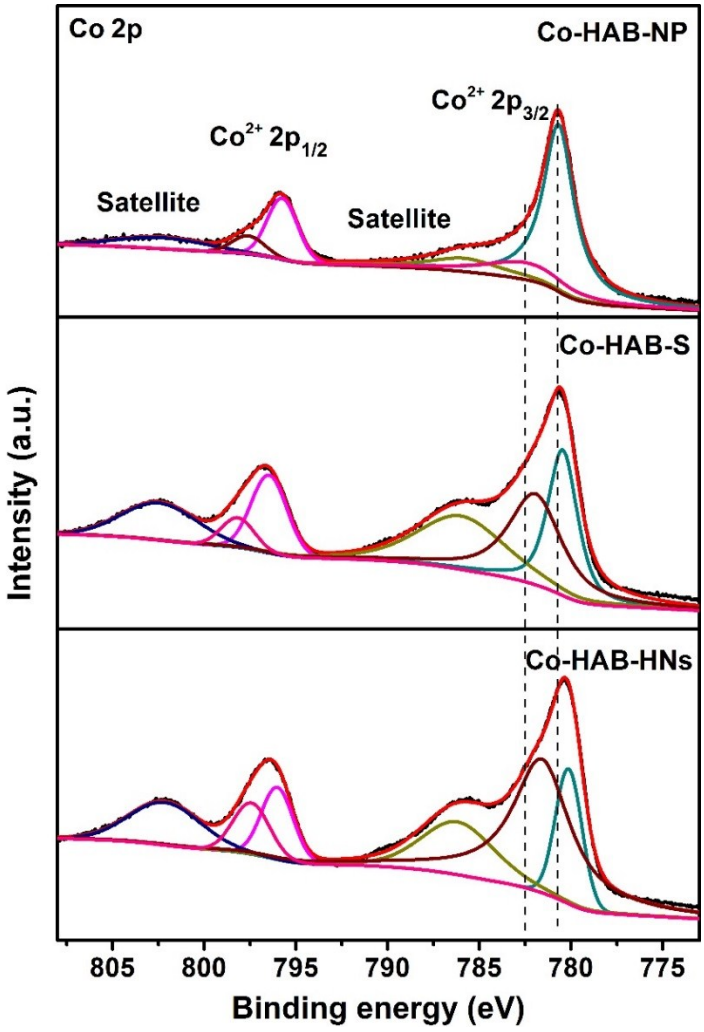

Figure S5 XPS spectra of Co 2p for Co-HAB-NP, Co-HAB-S and Co-HAB-HNs.

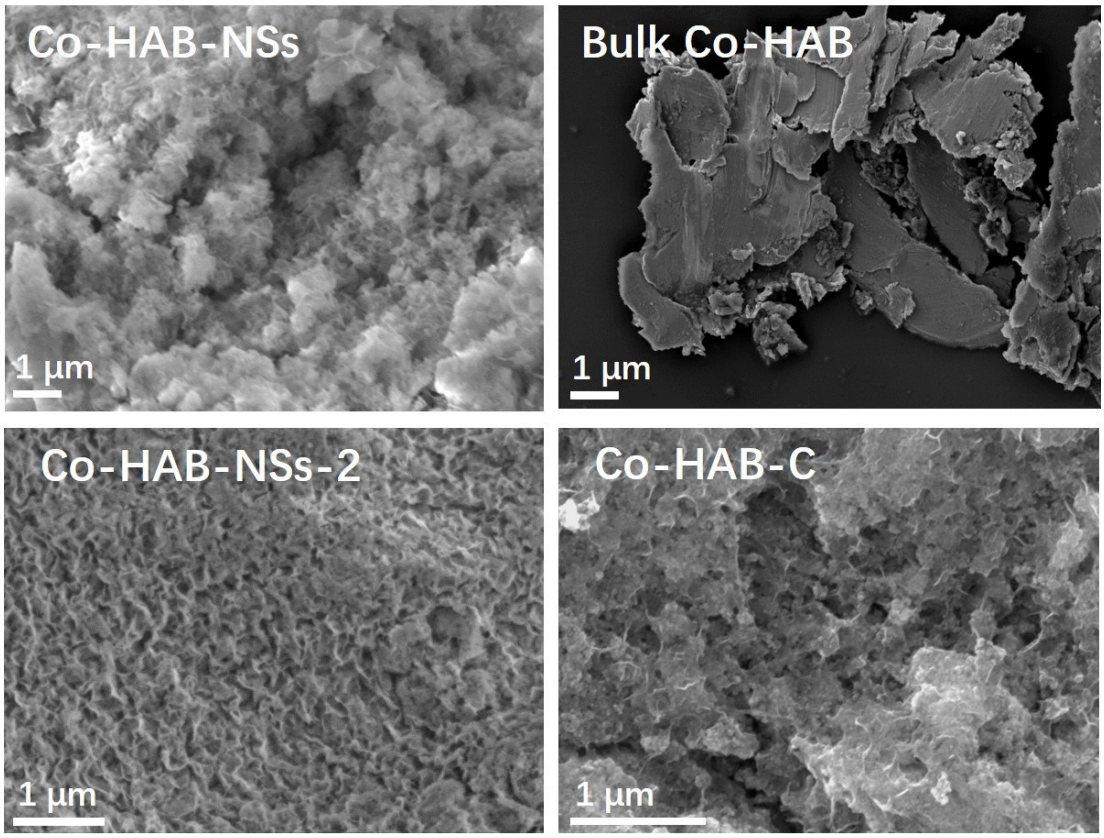

Figure S6. SEM images of Co-HAB-NSs, Co-HAB-NSs-2, Bulk Co-HAB and Co-HAB-C.

Co-HAB-NSs possesses much thinner nanosheets than Co-HAB-NSs-2 and presents a flower-like structure in which there are many gaps, whereas Co-HAB-NSs-2 displays a vertically aligned nanosheets array covering the whole plane with few space. Co-HAB-C displays a loose network than its procurer bulk Co-HAB.

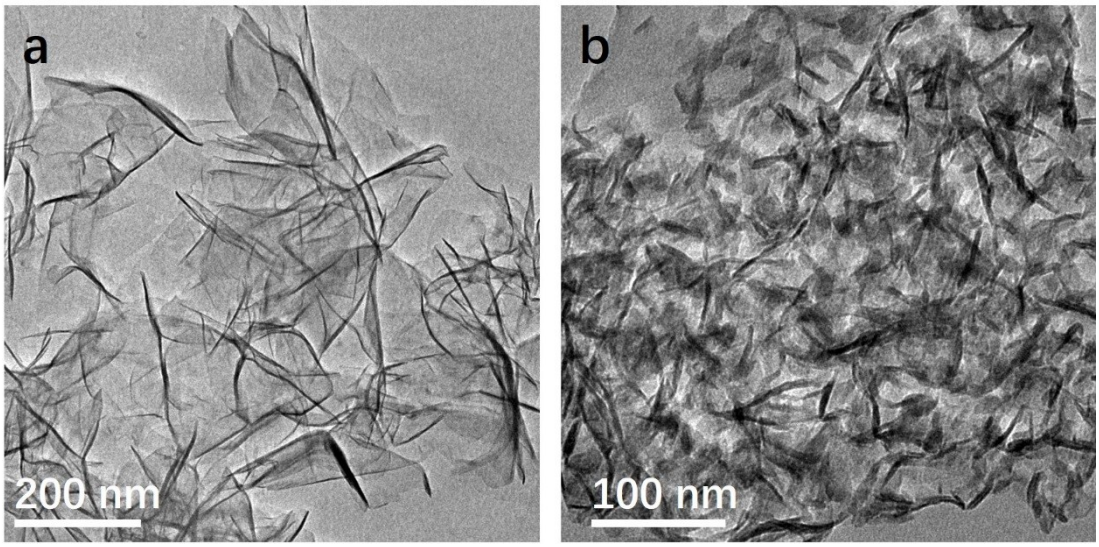

Figure S7. TEM images of (a) Co-HAB-NSs and (b) Co-HAB-NSs-2.

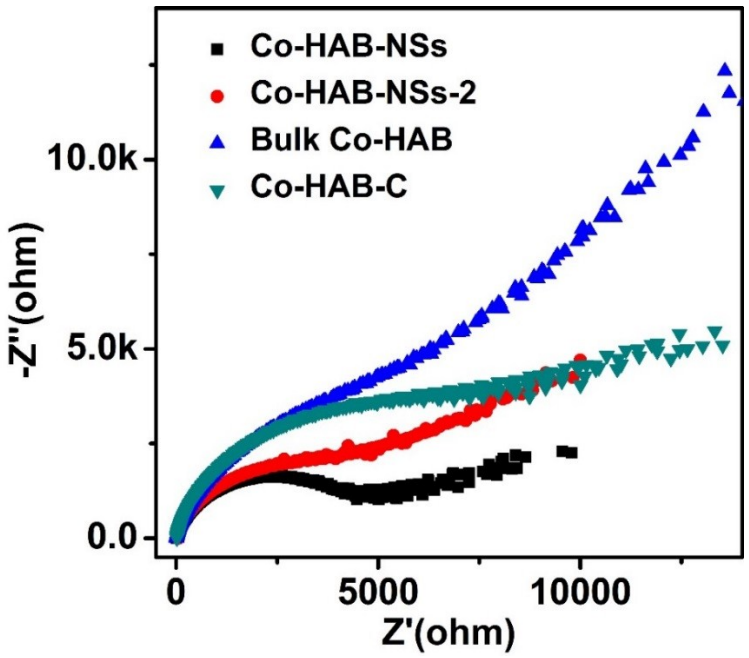

Figure S8. EIS curves of Co-HAB-NSs, Co-HAB-NSs-2, Bulk Co-HAB and Co-HAB-C.

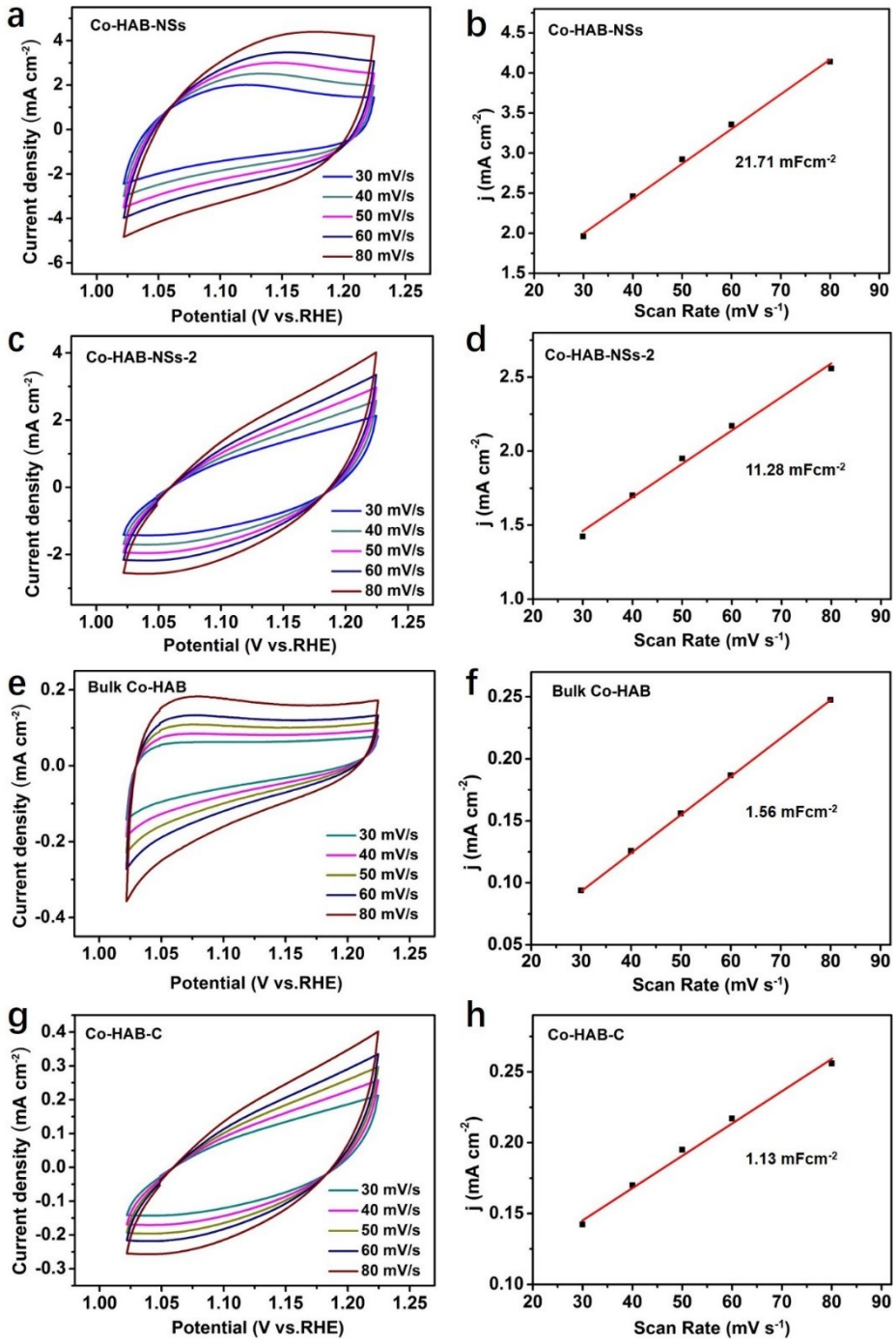

Figure S9. CV curves and double layer capacitance of Co-HAB-NSs, Co-HAB-NSs-2, Bulk Co-HAB and Co-HAB-C.

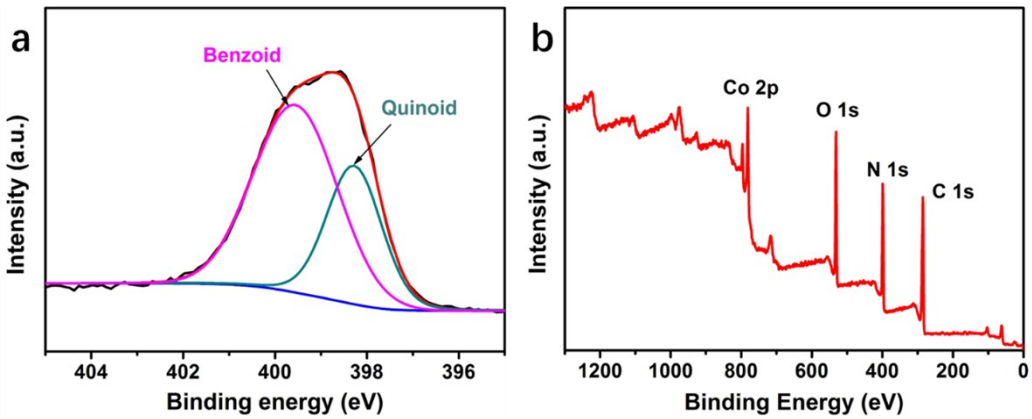

Figure S10. XPS spectra of (a) N 1s and (b) survey spectra for Co-HAB-UNs after long time electrolysis.

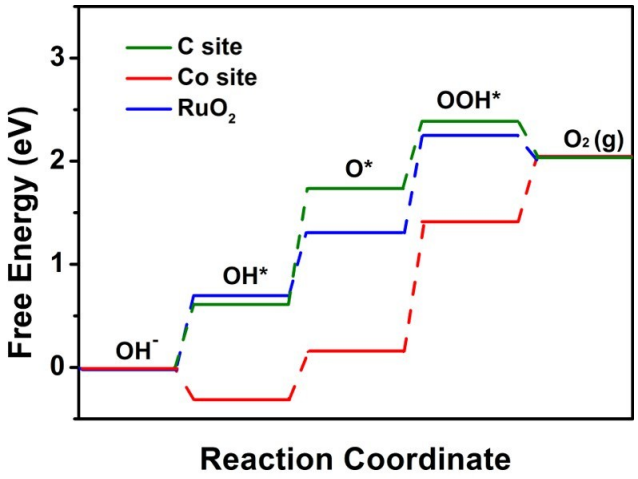

Figure S11. Free energy diagram of OER on Co-HAB and RuO_2 (110) surfaces. (U = 0.72 V)

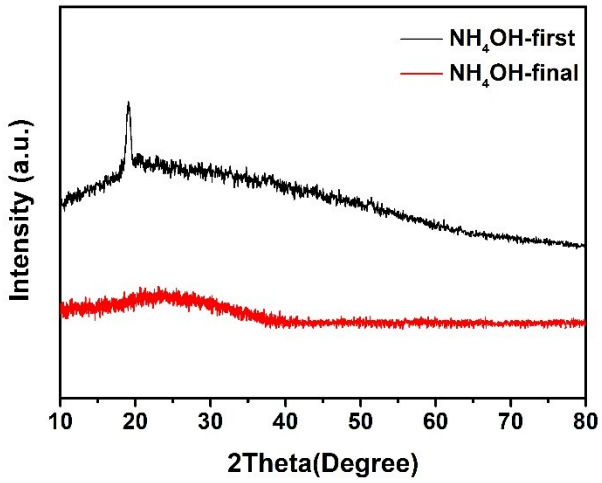

Figure S12 XRD patterns of NH_4OH-first and NH_4OH-final.

Table 1 Selected summary of the OER performance of recently reported Co-based electrocatalysts.

Catalysts	Electrolytes	Substrate	Overpotential (mV) at specific current density	Tafel slope (mV dec^{-1})	Ref.
CoPi	0.1 M KPi	ITO	410@1 mA cm^{-2}	62	[5]
CoCo-LDH	1 M KOH	GCE	350@10 mA cm^{-2}	45	[6]
Co_3O_4	1 M KOH	Au	400@10 mA cm^{-2}	49	[7]
$CoSe_2$ ultrathin nanosheets	0.1 M KOH	GCE	320@10 mA cm^{-2}	44	[8]
NiCo/NG	1 M KOH	GCE	~340@20 mA cm^{-2}	~111	[9]
Co–MOF nanosheets	1 M KOH	GCE	263@10 mA cm^{-2}	74	[10]
CoP/C	0.1 M KOH	GCE	360@10 mA cm^{-2}	66	[11]
α-$Co(OH)_2$-DS	1 M KOH	GCE	415@10 mA cm^{-2}	55	[12]
$Co(PO_3)_2$	0.1 M phosphate	GCE	440@8 mA cm^{-2}	74.1	[13]
crumpled graphene CoO	1 M KOH	GCE	340@10 mA cm^{-2}	71	[14]
NiCo DH	0.1 M KOH	Au	500@1 mA cm^{-2}	—	[15]
Co-HAB ultrathin nanosheets	**1 M KOH**	**GCE**	**310@10 mA cm^{-2}**	**56**	**This work**

Reference

1. G. Kresse and J. Hafner, *Physical Review B*, 1993, **47**, 558-561.

2. G. Kresse and J. Hafner, *Physical Review B Condensed Matter*, 1994, **49**, 14251-14269.

3. B. PE, *Phys Rev B Condens Matter*, 1994, **50**, 17953-17979.

4. G. Kresse and D. Joubert, *Phys.rev.b*, 1999, **59**, 1758-1775.

5. M. W. Kanan and D. G. Nocera, *Science*, 2008, **321**, 1072-1075.

6. F. Song and X. Hu, *Nat Commun*, 2014, **5**, 4477.

7. J. A. Koza, Z. He, A. S. Miller and J. A. Switzer, *Chemistry of Materials*, 2012, **24**, 3567-3573.

8. Y. Liu, H. Cheng, M. Lyu, S. Fan, Q. Liu, W. Zhang, Y. Zhi, C. Wang, C. Xiao, S. Wei, B. Ye and Y. Xie, *Journal of the American Chemical Society*, 2014, **136**, 15670-15675.

9. X.-R. Wang, J.-Y. Liu, Z.-W. Liu, W.-C. Wang, J. Luo, X.-P. Han, X.-W. Du, S.-Z. Qiao and J. Yang, *Advanced Materials*, 2018, **30**, 1800005.

10. Y. Xu, B. Li, S. Zheng, P. Wu, J. Zhan, H. Xue, Q. Xu and H. Pang, *Journal of Materials Chemistry A*, 2018, **6**, 22070-22076.

11. J. Ryu, N. Jung, J. H. Jang, H.-J. Kim and S. J. Yoo, *ACS Catalysis*, 2015, **5**, 4066-4074.

12. P. F. Liu, S. Yang, L. R. Zheng, B. Zhang and H. G. Yang, *Journal of Materials Chemistry A*, 2016, **4**, 9578-9584.

13. J. G. McAlpin, Y. Surendranath, M. Dincă, T. A. Stich, S. A. Stoian, W. H. Casey, D. G. Nocera and R. D. Britt, *Journal of the American Chemical Society*, 2010,

132, 6882-6883.

14. S. Mao, Z. Wen, T. Huang, Y. Hou and J. Chen, *Energy & Environmental Science*, 2014, **7**, 609-616.

15. Y. Feng, X.-Y. Yu and U. Paik, *Scientific Reports*, 2016, **6**, 34004.